10^{th} International Conference on Fracture Mechanics of Concrete and Concrete Structures
FraMCoS-X
G. Pijaudier-Cabot, P. Grassl and C. La Borderie (Eds)

A GRADIENT ENHANCED VISCOPLASTICITY-DAMAGE MICROPLANE MODEL FOR CONCRETE AT STATIC AND TRANSIENT LOADING

ALEXANDER FUCHS*, MICHAEL KALISKE†

*Institute for Structural Analysis, Technische Universität Dresden
01062 Dresden, Germany
e-mail: alexander.fuchs2@tu-dresden.de

†Institute for Structural Analysis, Technische Universität Dresden
01062 Dresden, Germany
e-mail: michael.kaliske@tu-dresden.de

Key words: Microplane model, Gradient Enhanced Damage, Viscoplasticity

Abstract. A microplane model is proposed to simulate the behavior of concrete at static and transient loading conditions. For that purpose, the model addresses several major characteristics in such loading scenarios by a coupled viscoplasticity-damage approach. The developed microplane yield function accounts for the realistic description of the different material responses in multiaxial tension and compression as well as the nonlinear material response at high volumetric pressure and the rate dependency of the concrete. Moreover, a penalty function to enable a stable and robust return mapping is developed. A damage approach considering proper stiffness degradation and crack closing effects is utilized. Furthermore, the model is regularized by an implicit gradient enhancement. The model is implemented within a 3D finite element code and the capabilities of the formulation are evaluated by several comprehensible numerical studies in comparison with experimental observations and results.

1 INTRODUCTION

Due to its heterogeneity, the material behavior of concrete has complex characteristics depending on the loading conditions. Thus, the computational modeling of concrete is challenging, especially in terms of finding a mathematical description of the material, which is able to consider the necessary properties concerning a particular application. The aim of this work is to propose a constitutive approach, which addresses the experimentally observed specific properties of concrete at triaxial static and transient loading. In particular for multiaxial loading, the strongly different material response at tension and compression loading is in the focus of this work. Furthermore, pore collapse of concrete at high volumetric pressure is considered as well as rate dependent behavior, which is essential for transient loading cases like impact scenarios. One highlight of the presented model is the plasticity formulation based on a rate depended modified three surface cap yield function with consideration of the third stress invariant and combined isotropic and cap hardening mechanisms. The degradation of the material is modeled by a plasticity driven damage approach, which distinguishes between tensile and compressive failure and allows the transition between these states. In order to overcome possible localization phenomena, a gradient enhancement of the damage approach is used. Both the plasticity and the damage formulation are implemented into a microplane framework to take into account the induced anisotropy of the material. The capabili-

ties and advantages of the model are shown and discussed by some examples.

2 MODEL FORMULATION

2.1 Microplane Framework

In the literature, several microplane models with different stress and strain projection approaches as well as constitutive laws are presented. Here, the model proposed in [1] is adopted, which is formulated in a thermodynamically consistent way. The model applies the kinematic constraint, i.e. the microplane strains are assumed to be equal to the projection of the macroscopic strain tensor to the microplanes. Furthermore, a volumetric-deviatoric (V-D) split of the microplane strain and stress quantities is utilized, with the corresponding projection tensors $\boldsymbol{V}$ and $\boldsymbol{Dev}$, respectively. Hence, the relation between the macroscopic strain tensor $\boldsymbol{\epsilon}$ and the microplane strains is given as

$$\epsilon_V = \boldsymbol{V} : \boldsymbol{\epsilon} \quad , \quad \boldsymbol{\epsilon}_D = \boldsymbol{Dev} : \boldsymbol{\epsilon}. \tag{1}$$

By decomposing the strains in an elastic and a plastic part and considering the damage by one damage parameter applied to both the volumetric and deviatoric stress parts, the stress strain relation reads

$$\begin{aligned}\boldsymbol{\sigma} =& \frac{3}{4\pi}\int_{\Omega}(1-d^{mic})[K^{mic}\boldsymbol{V}(\epsilon_V-\epsilon_V^{pl}) \\ &+ 2G^{mic}\boldsymbol{Dev}^T\cdot(\boldsymbol{\epsilon}_D-\boldsymbol{\epsilon}_D^{pl})]d\Omega,\end{aligned} \tag{2}$$

where K^{mic} and G^{mic} are the microplane bulk and shear moduli. Integration over the surface of the microplane unit sphere is achieved by a numerical integration scheme using 21 independent microplanes. The evolution of the plastic strains is described by the following flow rules

$$\dot{\epsilon}_V^{pl} = \dot{\lambda} m_V \quad , \quad \dot{\boldsymbol{\epsilon}}_D^{pl} = \dot{\lambda}\boldsymbol{m}_D, \tag{3}$$

where λ is the plastic multiplier. The corresponding flow directions m_V and $\boldsymbol{m}_D$ are derived from the microplane yield function f^{mic} as follows

$$m_V = \frac{\partial f^{mic}}{\partial \sigma_V} \quad , \quad \boldsymbol{m}_D = \frac{\partial f^{mic}}{\partial \boldsymbol{\sigma}_D}. \tag{4}$$

The microplane effective stresses are defined as

$$\sigma_V = K^{mic}\left(\epsilon_V - \epsilon_V^{pl}\right), \tag{5}$$

$$\boldsymbol{\sigma}_D = 2G^{mic}\left(\boldsymbol{\epsilon}_D - \boldsymbol{\epsilon}_D^{pl}\right). \tag{6}$$

The microplane bulk modulus K^{mic} and shear modulus G^{mic} can be derived from the from the macroscopic ones by

$$K^{mic} = 3K\,, \tag{7}$$

$$G^{mic} = G. \tag{8}$$

2.2 Smooth Rate dependent Microplane Cap Yield Function

In order to capture the complex triaxial behavior of concrete, a microplane yield function is proposed, which is based on the work of [2]. It consists of the adopted Drucker-Prager function expressed in terms of the microplane stresses and enhanced by a tension and compression cap. Moreover, the third stress invariant J_3 is considered in order to distinguish between triaxial tension, triaxial compression and shear loading states. The proposed yield function is shown in Fig. 1 and reads

$$f^{mic} = \frac{3}{2}\boldsymbol{\sigma}_D\cdot\boldsymbol{\sigma}_D - f_1^2\, f_t\, f_c + f_P, \tag{9}$$

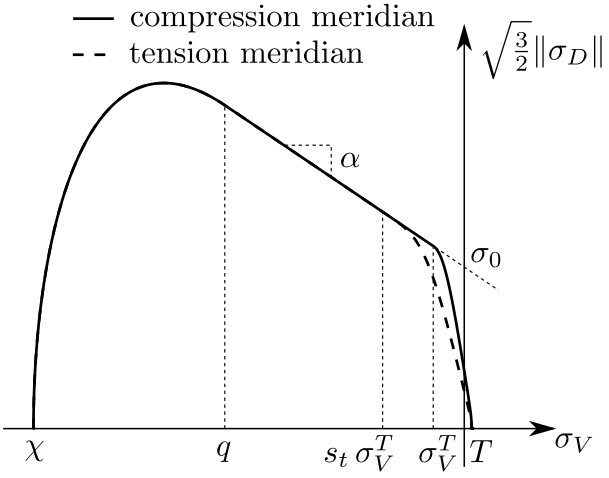

Figure 1: Initial smooth microplane cap yield function

where f_t and f_c are tension and compression caps, respectively. f_1 is the microplane Drucker-Prager function containing

the isotropic hardening function f_h and the rate dependent viscoplastic function f_{vp},

$$f_1 = \sigma_0 - \alpha\sigma_V + f_h(\kappa) + f_{vp}(\dot{\lambda}). \tag{10}$$

For the viscoplastic function, a consistency type formulation based on [3] is adopted,

$$f_{vp} = \eta_{vp}\dot{\lambda}, \tag{11}$$

where η_{vp} is a viscosity parameter. The isotropic hardening is linearly driven by the internal variable κ

$$f_h = D\kappa, \tag{12}$$

where D is a material constant. The evolution of κ is simply given as

$$\dot{\kappa} = \dot{\lambda}. \tag{13}$$

The compression cap is defined as

$$f_c = 1 - H_c\,(q - \sigma_V)\,\frac{(\sigma_V - q)^2}{X^2}, \tag{14}$$

$$X = R\,f_1(q), \tag{15}$$

where R is the volumetric-deviatroric axis ratio. q is an internal variable describing the intersection point between the Drucker-Prager function and the compression cap with an initial value σ_V^C being a material constant. Moreover, q drives the movement of the compression cap, called cap hardening. The cap hardening describes the densification of the concrete due to pore collapse at high volumetric pressure according to the Hugoniot curve of the material. Especially, at high dynamic loading conditions, where inertia induced high confinement pressures may occur, this densification process has a strong influence on the wave propagation in the material and is the reason for the evolution of shockwaves. The Hugoniot curve basically describes the nonlinear relation between volumetric strains and volumetric pressure. Here, the Hugoniot curve for concrete is approximated by

$$\epsilon_V^{pl} = h_q(q) = W(e^{D_1(\chi(q)-\chi_0)} - 1), \tag{16}$$

where W is the maximum plastic volumetric strain at hydrostatic compression and D_1 is a material constant. χ and χ_0 are the current and initial volumetric abscissa of the cap, respectively. Therefore, the internal variable q increases according to the evolution law

$$\dot{q} = \dot{\lambda}\,H_c\frac{\partial f^{mic}}{\partial\sigma_V}\frac{\partial h_q}{\partial q} = \dot{\lambda}m_q. \tag{17}$$

The tension cap defined as

$$f_t = 1 - H_t\left(\sigma_V - s_t\,\sigma_V^T\right) \cdot \left(\frac{\sigma_V - s_t\,\sigma_V^T}{T - s_t\,\sigma_V^T}\right)^{2+A\frac{\sigma_V^e - \sigma_V^T}{T-\sigma_V^T}}, \tag{18}$$

$$T = T_0 + R_t f_h(\kappa) + f_{vp}(\dot{\lambda}), \tag{19}$$

where σ_V^T, R_t, T_0 and A are material parameters. σ_V^T is the initial abscissa of the intersection point between the tension cap and the Drucker-Prager yield function, and T_0 is the initial intersection of the tension cap with the volumetric axis. Due to hardening and rate effects, the current intersection point T increases, where this increase is controlled by the parameter R_t. A is a shape parameter controlling the steepness of the cap. The Heavyside functions H_c and H_t are defined as

$$H(x) = \frac{1}{2}(1 + \mathrm{sign}(x)), \tag{20}$$

activating the particular caps when the stress state is within their domain. The scaling function s_t moves the initial intersection point σ_V^T depending on the triaxial loading conditions quantified by the third stress invariant J_3 and the Lode angle

$$\theta = \frac{1}{3}\cos^{-1}\left(\frac{3\sqrt{3}\,J_3}{2\,J_2^{3/2}}\right), \tag{21}$$

calculated from the macroscopic stress tensor of the previous time step. This formulation enables a shaping of the cross-section of the yield function. Here, the Willam-Warnke approach for shaping the cross-section [4] is adopted and the Lode angle dependent radius of the cross-sections reads

$$r(\theta) = [2(1-e^2)\cos(\theta) + (2e-1)\sqrt{4(1-e^2)\cos^2(\theta) + 5e^2 - 4e}] / [4(1-e^2)\cos^2(\theta) + (2e-1)^2], \tag{22}$$

where $0.5 \leq e \leq 1$ is an eccentricity parameter. However, the scaling function for shaping the cross-section is given as

$$s_t = -\frac{T_0}{\sigma_V^T}\left(\frac{1}{r^2\, r_0} - 1\right)^{1/s_{t0}}, \tag{23}$$

$$s_{t0} = 2 + A\frac{-\sigma_V^T}{T_0 - \sigma_V^T}, \tag{24}$$

$$r_0 = 1 - \left(\frac{-\sigma_V^T}{T_0 - \sigma_V^T}\right)^{s_{t0}}. \tag{25}$$

Since, the shaping of the cross-section is realized by the movement of the intersection point between the Drucker-Prager function and the tension cap, the influence of the scaling function decreases with increasing volumetric stresses and vanishes in the intersection point. That means, the Drucker-Prager part and the compression cap have always a circular cross-section. s_t is constructed in such a way, that the cross-section in the π-plane is forced to be exactly the in $r(\theta)$ prescribed shape. However, the proposed mathematical formulation of the tension cap might lead to non physical results, because it creates a second domain of valid stress states as an adverse side effect, which allows stress states with higher volumetric stresses than T. In order to suppress this non physical domain, a penalty function is added to the yield function and defined as follows

$$f_P = -P\, H_P(\sigma_V - T)\,(\sigma_V - T)^2, \tag{26}$$

where P is a penalty parameter.
Due to the multiplicative coupling of the Drucker-Prager function and the proposed cap functions, a smooth C^1-continuous microplane yield surface is achieved, which offers several numerical advantages.

2.3 Damage Evolution

Modeling the damage initiation and evolution of concrete at cyclic loading, it is necessary to consider the different damage characteristics in tension and compression as well as the transition between these states. Here, a damage model introduced in [1] is used, which decomposes the effective damage d^{mic} into a compression d_c^{mic} and a tension part d_t^{mic} as follows

$$1 - d^{mic} = (1 - d_c^{mic})(1 - r_w d_t^{mic}), \tag{27}$$

where both parts are driven by an exponential evolution law

$$d_t^{mic} = 1 - \exp(-\beta_t \gamma_t^{mic}), \tag{28}$$

$$d_c^{mic} = 1 - \exp(-\beta_c \gamma_c^{mic}). \tag{29}$$

β_t and β_c are material constants. r_w is the split weight factor describing the transition between tension and compression states and is defined as

$$r_w = \frac{\sum_{I=1}^{3} \left\langle \epsilon^I \right\rangle}{\sum_{I=1}^{3} |\epsilon^I|}, \tag{30}$$

where $\left\langle \epsilon^I \right\rangle$ is the positive part of the I-th macroscopic principal strain. The rate of the equivalent strains is a function of the volumetric plastic strain rate as follows

$$\dot{\eta}_t^{mic} = \begin{cases} r_w \dot{\epsilon}_V^{pl} & \dot{\epsilon}_V^{pl} > 0 \\ 0 & \dot{\epsilon}_V^{pl} \leq 0 \end{cases}, \tag{31}$$

$$\dot{\eta}_c^{mic} = \begin{cases} (1 - r_w)\dot{\epsilon}_V^{pl} & \dot{\epsilon}_V^{pl} > 0 \\ 0 & \dot{\epsilon}_V^{pl} \leq 0 \end{cases}. \tag{32}$$

2.4 Implicit Gradient Regularization

The implicit gradient enhancement can be seen as a regularization method in order to overcome localization issues by a spatial averaging of a local variable. This averaged value is considered as an extra nonlocal degree of freedom and described by a partial differential equation in addition to the balance of linear momentum. Hence, the strong coupled field problem reads

$$\nabla \cdot \boldsymbol{\sigma} + \boldsymbol{f} = 0, \tag{33}$$

$$\bar{\eta}_m - c\nabla^2 \bar{\eta}_m = \eta_m, \tag{34}$$

where $\boldsymbol{\sigma}$ is the Cauchy stress tensor and $\boldsymbol{f}$ is the body force vector. The nonlocal interaction is controlled by the gradient parameter c. Moreover, homogeneous Neumann boundary conditions are applied to the nonlocal field. The evolution of the nonlocal variable $\bar{\eta}_m$ is driven by its local counter counterpart η_m as a source term. Here, the local variables are

$$\eta_m = \begin{bmatrix} \eta_{mt} \\ \eta_{mc} \end{bmatrix} = \begin{bmatrix} \frac{1}{4\pi}\int_\Omega \eta_t^{mic} d\Omega \\ \frac{1}{4\pi}\int_\Omega \eta_c^{mic} d\Omega \end{bmatrix}, \tag{35}$$

which causes two extra degrees of freedom. In order to achieve a full regularization of plastic damage models an over-nonlocal formulation is utilized, where the over-nonlocal variable $\hat{\eta}^{mic}$ is defined as a linear combination of the respective local and nonlocal variable

$$\hat{\eta}_t^{mic} = m\bar{\eta}_{mt} + (1-m)\eta_t^{mic}, \qquad (36)$$

$$\hat{\eta}_c^{mic} = m\bar{\eta}_{mc} + (1-m)\eta_c^{mic}. \qquad (37)$$

In order to achieve regularization, the material constant m should be larger than 1. This enhanced variables are used to drive the damage in Eqs. (28) and (29) as follows

$$\gamma_t^{mic} = \begin{cases} \hat{\eta}_t^{mic} - \gamma_{t0} & \hat{\eta}_t^{mic} > \gamma_{t0} \\ 0 & \hat{\eta}_t^{mic} \leq \gamma_{t0} \end{cases}, \qquad (38)$$

$$\gamma_c^{mic} = \begin{cases} \hat{\eta}_c^{mic} - \gamma_{c0} & \hat{\eta}_c^{mic} > \gamma_{c0} \\ 0 & \hat{\eta}_c^{mic} \leq \gamma_{c0} \end{cases}, \qquad (39)$$

where γ_{t0} and γ_{c0} are damage treshold for tension and compression, respectively.

3 NUMERICAL VERIFICATION

Before applying the proposed model in the simulation of a complex structure, it makes sense to analyze and verify the characteristics of the formulation in comprehensible numerical test simulations. For that purpose, a series of single element studies addressing different properties of the model are performed and evaluated.

3.1 Uniaxial Tests

In Fig. 2, the results of a quasi-static displacement controlled single element, loaded cyclicly in tension and compression, are shown. It can be seen that the first cycles in the tension domain and especially the stiffness degradation of the material, are in a good agreement with the experiments of [5]. Furthermore, the model is able to consider stiffness recovery when switching from the tension to the compression domain, due to crack closing. By increasing the compressive load, the compression part of the damage starts to evolve and the concrete undergoes compressive failure. It is worth noticing, that these characteristics are exemplary shown in a uniaxial testcase, but they are also considered at multiaxial loading conditions. The described properties are important for both static and transient loading scenarios. Especially under wave propagation, the material experiences cyclic loading conditions in tension and compression.

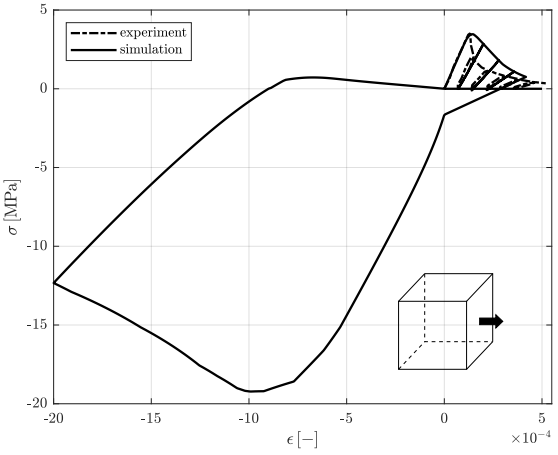

Figure 2: Cyclic tension compression transition at uniaxial loading compared to cyclic uniaxial tension experiments of Karsan et al. [5]

3.2 Multiaxial and Hydrostatic Tests

In this section, the behavior of the microplane model at multiaxial loading is presented. Since the different microplanes are independent of each other, the macroscopic or effective yield envelope cannot directly be derived from the microplane yield function. Therefore, a single element is loaded at several discrete monotonic biaxial and triaxial stress paths until the material starts to soften. Fig. 3 shows the biaxial yield envelope ($\sigma_3 = 0\,\text{MPa}$) of the model in comparison to the experiments of [6].

The yield envelope at triaxial loading is exemplarily shown for pure deviatoric loading ($\sigma_V = 0\,\text{MPa}$) in the π-plane in Fig. 4. The plotted value $r(\theta)$ describes the ratio between the octahedral peak stresses at a certain Lode angle θ and the octahedral peak stresses at triaxial compression ($\theta = 60°$). It is obvious, that the triaxial envelope follows the predefined shape

from Eq. (22) as desired. It can also be seen, that the eccentricity parameter e describes the reduction factor of the octahedral peak stresses in triaxial tension ($\theta = 0°$). It should be noticed, that the formulation of the model is designed in a way, that the triangular shape of the cross-section of the macroscopic yield envelope reduces with increasing volumetric pressure, in order to achieve a better agreement with the experiments of [6] in the compression domain.
These examples show the capability of the model to capture the different behavior at multiaxial tension and compression, which is one of the most prominent characteristics of concrete.

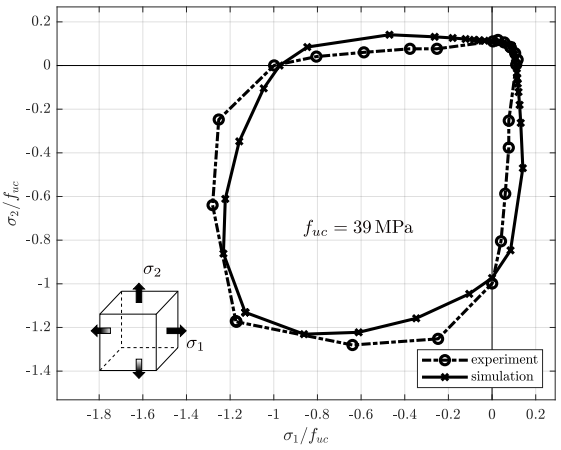

Figure 3: Biaxial yield envelope compared to experimental results of Lee et al. [6]

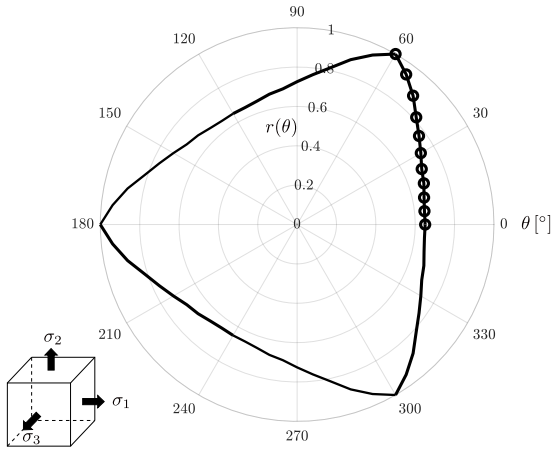

Figure 4: Yield envelope at triaxial loading conditions in the pure deviatoric π-plane ($\sigma_V = 0\,\mathrm{MPa}$)

Since concrete is a porous material, it crushes at high hydrostatic pressure by the collapse of the pores. Crushing and the accompanying densification of the material lead to a nonlinear volumetric response as it is experimentally observed in [7]. This nonlinear behavior is described by the hardening evolution law of the compression in Eqs. (16) and (17). Fig. 5 shows the response of the model in a cyclic hydrostatic test in comparison to the experiment of [7]. Especially in transient analysis, where inertia effects lead to high volumetric pressure, the nonlinear behavior of the crushed material induces shockwaves as it is described in [8].

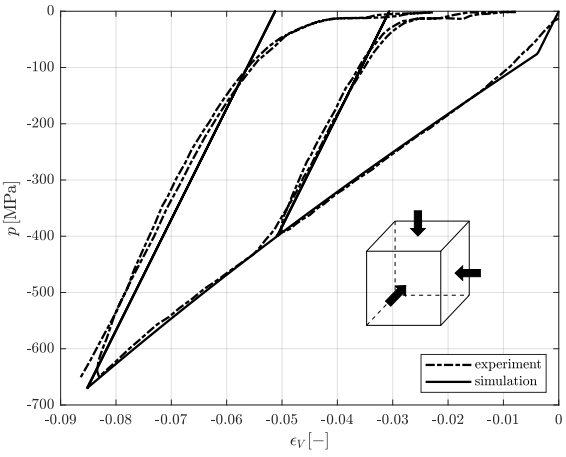

Figure 5: Model response at hydrostatic pressure compared to experimental results of Gabet et al. [7]

3.3 Rate Dependency

The influence of the loading rate is investigated in monotonic uniaxial tension tests at different strain rates. In Fig. 6, the variation of the stress-strain relation for seven different strain rates is shown. It can be seen, that the peak stress and strain increase at increasing strain rate. This increase is a result of the viscoplastic formulation of the proposed model leading to a decreased evolution of the plastic strains and, therefore, a delayed damage evolution. One can also see, that the viscoplastic response converges to the linear elastic case at increasing strain rate, which is a major difference compared to viscoelastic approaches. The results show the capability of the model to consider the

strength increase of concrete at dynamic loading. It is worth noticing, that the calibration and validation of the viscoplastic formulation should be done on the structural level, since the dynamic strength increase is influenced by many effects like inertia and size effects.

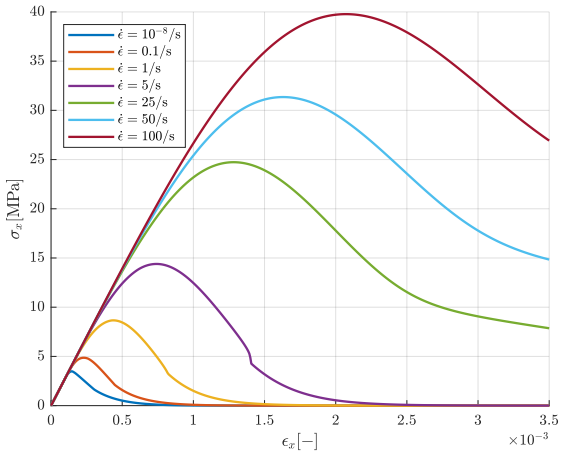

Figure 6: Stess strain response for different strain rates at uniaxial loading

4 CONCLUSIONS

In this contribution, a constitutive model for plain concrete is presented. The model addresses several key properties for a realistic description of the material. First, the model is formulated in terms of the microplane approach, which can capture the induced anisotropy by independent evaluation of the different microplanes. Second, a newly designed smooth rate dependent microplane cap yield function with combined isotropic and cap hardening mechanisms is introduced. This plasticity formulation coupled with the proposed gradient damage approach provides a realistic and robust description of the major characteristics at multiaxial static and transient loading scenarios. By the consideration of the third stress invariant, the different behavior of concrete at multiaxial tension and compression can be captured. The introduced cap hardening mechanism allows the consideration of the nonlinear volumetric behavior at high hydrostatic pressure according to the Hugoniot curve of the material. In order to consider the rate dependent response of concrete, a consistency type viscoplasticity approach is used. Moreover, the introduced penalty function and the smoothness of the overall yield function enable a stable return mapping and tangent modulus. The utilized damage split is able to describe the tension compression transition with the accompanying stiffness recovery. This makes the model suitable for general cyclic loading cases.
The proposed constitutive formulation is analyzed and verified by comprehensible single element test simulations investigating the performance of the model regarding the addressed characteristics of concrete. The results of this study are compared to corresponding experimental results and observations in the literature. In general, the model gives the desired behavior and is in good agreement with the experiments. Since the model captures several major characteristics of concrete, concerning multiaxial static and transient loading cases, it is very promising to proceed and validate it on the structural level. These studies will also show the capability of the introduced implicit gradient enhancement to regularize the model and to eliminate mesh sensitivity caused by the strain softening constitutive formulations.

5 ACKNOWLEDGEMENTS

This work is supported by the German Research Foundation (DFG) within Research Training Group GRK 2250, Project B3.

REFERENCES

[1] Zreid, I. and Kaliske, M. 2018. A gradient enhanced plasticity–damage microplane model for concrete. *Computational Mechanics* **62**:1239–1257.

[2] Schwer, L. E. and Murray, Y. D. 1994. A three-invariant smooth cap model with mixed hardening. *International Journal for Numerical and Analytical Methods in Geomechanics* **18**:657–688.

[3] Wang, W. M., Sluys, L. J. and De Borst, R. 1997. Viscoplasticity for instabilities due

to strain softening and strain-rate softening. *International Journal for Numerical Methods in Engineering* **40**:3839–3864.

[4] Willam, K. J. and Warnke, E. 1975. Constitutive model for the triaxial behaviour of concrete. *Proc. Intl. Assoc. Bridge Structl. Engrs* **19**:1–30.

[5] Karsan, I. D., and Jirsa, J. O. 1969. Behavior of concrete under compressive loadings. *Journal of the Structural Division* **95**:2543–2563.

[6] Lee, S. K. Song, Y. C., and Han, S. H. 2004. Biaxial behavior of plain concrete of nuclear containment building. *Nuclear Engineering and Design* **227**:143–153.

[7] Gabet, T., Malécot, Y., and Daudeville, L. 2008. Triaxial behaviour of concrete under high stresses: Influence of the loading path on compaction and limit states. *Cement and Concrete Research* **38**:403–412.

[8] Meyers, M. A. 1994. *Dynamic behavior of materials,* John Wiley & Sons, New York